Tough, Waterproofing, and Sustainable Bio-Adhesive Inspired by the Dragonfly Wing

Ying Zhou, Jing Luo, Qiumei Jing, Shengbo Ge,* Sherry Chen, Zhanhu Guo, Jianzhang Li,* Zixiao Liu, Ping He, Ximin He,* and Ben Bin Xu*

The development of multifunctional bio-adhesive plays a critical role in achieving a sustainable society, where the intrinsic sensitivity to water and poor dynamics severely bottlenecks its scale-up application. Inspired by the microstructure of dragonfly wings, a strong and tough adhesive with excellent reprocessability is designed and developed by creating a dynamic network consisting of a lignin polyurea (LPU) framework with soybean protein (SP). The LPU framework act as the rigid nervures to slow crack propagation and transfer stress, while the SP dissipate the strain energy through the interplay from the graded hydrogen and imine bonds generated between LPU and SP. The bio-adhesive achieves significant enhancements in fracture toughness and water resistance by ≈7 and 23 folds, respectively, compared with SP. Furthermore, the capacity for diffusion and restoration of dynamic network endows the adhesive with superior reprocessability, enabling recycled particleboard to achieve high retention of modules (over 80%). This sustainable bio-adhesive approach offers a promising eco-friendly alternative to the conventional petrochemical adhesive.

1. Introduction

Adhesive plays an indispensable role across various engineering disciplines, such as smart buildings, aerospace, and automotive engineering.[1] The current adhesive market has been predominantly occupied by petroleum-derived products, which lead to increasing concerns on environmental sustainability.[2]

The innovation of next-generation adhesives with sustainable materials holds great promises to mitigate these environmental impacts.[3] Natural protein,[4] lignin,[2a] polysaccharides[5] and other polymers are considered sustainable materials with potential applications to replace existing petroleum-derived polymers. The design of sustainable adhesives involves modifying material variables (e.g., chain stiffness, intermolecular interactions, entanglement, and crystallinity) to facilitate high strong and toughness,[6] but this is often at the expense of high diffusivity and dynamic interactions.[7] Recent advancements in incorporation of dynamic covalent[8] and non-covalent interactions[9] have been utilized to simultaneously improve material strength, toughness, and reprocessability. However, bio-based materials with reversible supramolecular cross-linking usually show certain technical disadvantages such as decayed mechanical properties or loss of adhesion in the aqueous environment,[10] which remain yet to be resolved.

In general, it is difficult to produce adhesives with both excellent load-bearing capacity and fracture resistance, as the strength and toughness can hardly co-exist in of the same material.[11] Natural materials with unique hierarchical structures offer enormous potential to overcome such conflict.[12] For example,

Y. Zhou, J. Luo, S. Ge, J. Li
Co-Innovation Center of Efficient Processing and Utilization of Forest
Resources, College of Materials Science and Engineering
Nanjing Forestry University
Longpan Road 159, Xuanwu District, Nanjing 210037, China
E-mail: geshengbo@njfu.edu.cn; lijzh@bjfu.edu.cn
Y. Zhou
Department of Materials Science and Engineering
National University of Singapore
Singapore 117575, Singapore

Q. Jing, S. Chen, Z. Guo, B. B. Xu
Department of Mechanical and Construction Engineering
Faculty of Engineering and Environment
Northumbria University
Newcastle Upon Tyne NE1 8ST, UK
E-mail: ben.xu@northumbria.ac.uk
J. Li
State Key Laboratory of Efficient Production of Forest Resources & MOE
Key Laboratory of Wood Material Science and Application
Beijing Forestry University
Qinghua East Road 35, Haidian District, Beijing 100083, China
Z. Liu, P. He, X. He
Department of Materials Science and Engineering
University of California Los Angeles (UCLA)
Los Angeles, CA 90095, USA
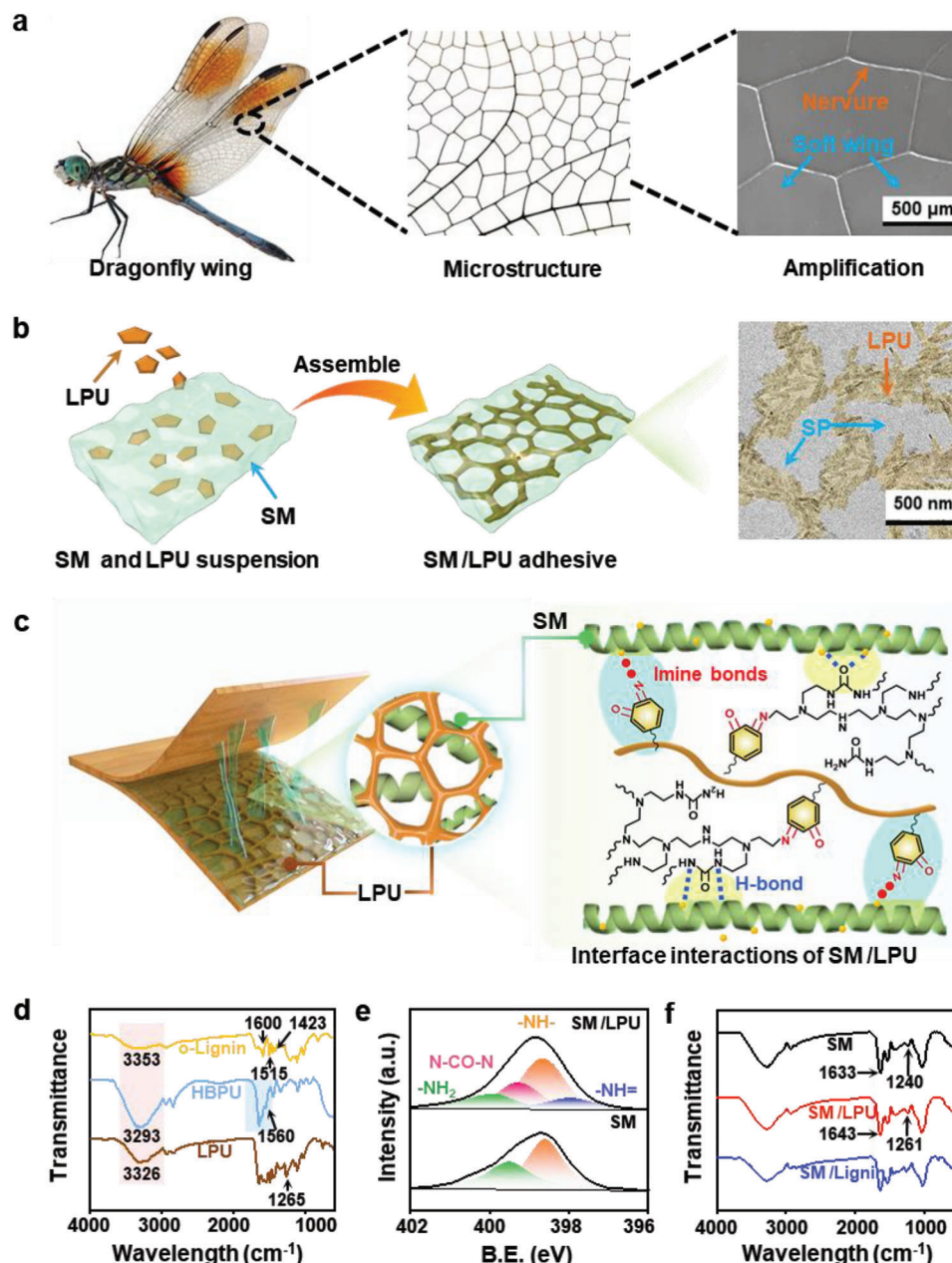E-mail: ximinhe@ucla.edu

Figure 1. Multi-length scale design strategy for the bio-mimetic adhesive. Illustration of a) Dragonfly wing pattern with microscopic morphology; b) the nanostructure of composite consisting of LPU skeleton and SP matrix; c) the dynamic imine bonds and H-bonds interaction between SP and interwoven network of LPU. FT-IR results of d) LPU; f) SP/LPU. e) The N1s of XPS spectrum of SP/LPU.

bio-inspired adhesives with micro-/nano-structures have been found with unique dissipate mechanisms, such as those inspired by pearl layers,[13] spider silk,[14] and insect cuticle.[15] Dragonfly wing (**Figure 1a**) has a fascinating pattern consisting of a soft wing membrane and rigid nervures,[16] where the rigid nervures act as a reinforcing skeleton to transfer stress and resist mechanical deformation, and the soft wing membrane around the nervures plays a key role in strengthening the dissipated stress energy.[17] Due to the highly organized hierarchical structure and special breaking mechanism, dragonfly wings have excellent toughness and load-bearing capacity.[18] Therefore, inspired by

the microscopic structure of dragonfly wings and the strengthening and toughening mechanism, the energy dissipation path in the adhesive can be deliberately designed, which has great potential for manufacturing tough adhesives.

Lignin molecules wrapped around fibers can covalently associate with hemicellulose, generating a 3D interwoven structure with cellulose fibers in wood. Lignin is the most abundant renewable natural phenolic polymer on the planet.[19] In addition to its good water resistance and antimicrobial properties, lignin serves as an ideal choice for the rigid skeleton in adhesives.[20] However, the reactivity of lignin is generally limited due to its high

**ADVANCED
SCIENCE NEWS**

www.advancedsciencenews.com

**ADVANCED
FUNCTIONAL
MATERIALS**

www.afm-journal.de

molecular weight, complex structure, small number of active groups, and large steric hindrance.[21] To enhance its interfacial interactions with matrix, the self-assembly based on donor–acceptor (D–A) hydrogen bonding is usually introduced. Moreover, the D–A hydrogen bonds can offer urea groups with reversible intramolecular interactions and heat-driven reassembly[22] to address the challenge of low reprocessability due to poor chain mobility.[23] Polyurea networks assembled through this method are not only extremely stable, but also exhibit excellent self-healing, complementation, and recognition capabilities.[24] Zhang et al. employed urea groups to deliver dynamic covalent networks,[25] to achieve high strength, ductility and toughness, and reprocessability. The diamide structure of urea moiety represents one of the most stable hydrolysis-resistant chemical bonds,[26] making a chemically active urea backbone a sensible choice to reach strength-toughness balance and facilitate good reprocessability and water resistance through the effective chain diffusion functions.

In this work, we design and develop a bio-adhesive with a double cross-linked network inspired by the dragonfly wing. The network contains a lignin polyurea (LPU) rigid skeleton pattern and a soybean protein (SP) based energy-absorbing units. The double cross-linking network through dynamic imine and hydrogen bonds maximize the strong interplay between LPU and SP (Figure 1b,c). The resulted structural bio-adhesive presents a rich set of bespoke features such as good mechanical properties (strength and toughness), superior reprocessability, excellent durability, good waterproof property, optimal antimicrobial property, and scaling-up capability.

2. Results and Discussion

2.1. The Design, Fabrication, and Characterization of Structural SP/LPU Adhesive

To construct the desired SP/LPU cross-linking network, first, we modify lignin using hyperbranched polyuria (HBPU) to construct and regulate aggregation density of hydrogen bonds between the LPU and the SP matrix. The LPU (Figure S1, Supporting Information) is synthesized by using Fe^{3+} to oxidize the lignin to produce redox-active semiquinone/quinone (o-lignin, Figure S2, Supporting Information).[27] The hyperbranched polyurea (HBPU, Figure S3, Supporting Information) is subsequently grafted and anchored on lignin to generate LPU. The successful synthesis of LPU is verified by FT-IR spectra in Figure 1d. The absorption peaks of LPU at 1600, 1515, and 1423 cm^{-1} are attributed to the vibration of aromatic rings in lignin.[28] Compared to HBPU, the N—H bending vibration peaks of —CO—NH$_2$ and —NH—CO—NH— at 1560 cm^{-1} moved to 1550 cm^{-1}, which are caused by Schiff reaction between the amino group of HBPU and the quinone of o-lignin. The fitted XPS spectra of LPU (Figure S4, Supporting Information) confirm the successful introduction of HBPU on lignin with the cross-linking of imine.

The urea-based sequences on LPU backbone provide abundant hydrogen bonding donors and acceptors. The signature peaks of lignin for stretching vibrations of —OH (3353 cm^{-1}) and C=O (1697 cm^{-1}) are found to shift to 3326 and 1642 cm^{-1} in LPU (Figure 1d), indicating amide–amide and amide-carbonyl hydro-

gen bond-driven self-assembly.[29] The unique dendritic structural character of HBPU allows individual LPU nanosheets to be scaffolded to prevent aggregation. The TEM results (Figure S5, Supporting Information) reveal the structure of LPU as precursors for the simulated "neural" framework. Meanwhile, The zeta potential of LPU nanosheets is −24 mV (Figure S6, Supporting Information), which further indicates the nanosheets dispersing uniformly stable.

Lignin-based modification and dispersion are the prerequisites for assembling the ordered pattern. The distribution morphology of the SP/LPU suspension under optical microscope, as shown in Figure S7 (Supporting Information). The SP is irregular spherical particle, and due to the color of the LPU, it is observed that some darker portions are uniformly distributed around the SP, and the TEM results of the SP/LPU pattern (Figure 1b) identified the SP wrapped around the LPU nanosheets. In contrast, the SP/Lignin suspension shows a chaotic lignin aggregation pattern, which is precisely due to the lack of effective interfacial force between lignin and SP. According to the principle of self-assembly of nanomaterials, intermolecular forces are the main reason for the formation of this structure. Due to the strong electronegativity of LPU, the nanosheets are directionally distributed around the negatively charged SP (−3 mV) particles through electrostatic repulsion. In addition, the branching of LPU with multiple active sites enables HBPU molecules to trap and bind SP chains through interfacial interactions, maximizing the bonding chance between the hydrogen-bonding sites and easy to form high-density hydrogen bonds.

The interfacial supramolecular interactions between LPU and SP are illustrated in Figure 1c and further assessed by XPS spectra (Figure 1e). It can be found that SP contains absorption peaks at 399.5 and 398.5 eV in the N 1s region, corresponding to —NH$_2$ and —NH—, respectively. The SP/LPU result shows new peaks at 399.3 and 398 eV, corresponding to —N—CO—N— and —NH=, respectively. Meanwhile, the peaks of —NH$_2$ and —NH— shift to the higher binding energy region to 398.7 and 400 eV, which proves the existence of cross-linking mechanism of imine bond between SP and LPU and the formation of polyurea network. The FT-IR results (Figure 1f) present the characteristic peaks of O—H/N—H, C=O for SP at 1633 and 3276 cm^{-1}.[30] The blueshift of SP/LPU at C=O stretching and the decreases in the absorption intensity of —N—H stretching affirms the strong H-bonding interactions between C=O and N—H of SP and urea groups in LPU. The storage modulus of SP/LPU (Figure S8, Supporting Information) is significantly higher than that of SP, indicating the increase in interfacial strength and mechanical properties.[31] Therefore, electrostatic repulsion and interfacial force are the important reasons for inducing the self-assembly of LPU nanosheets around SP microspheres into a uniformly distributed mesh network pattern to form this morphology.

2.2. Adhesion and Water Resistance of SP/LPU Adhesives

We evaluate the adhesion of SP/LPU on plywood products by tensile shear test (corresponding to mode II fracture, **Figure 2a**).[32] The SP adhesives bonded three-layer plywood undergo control tests with dry state and state after immersing at 63 °C hot

**ADVANCED
SCIENCE NEWS**

www.advancedsciencenews.com

**ADVANCED
FUNCTIONAL
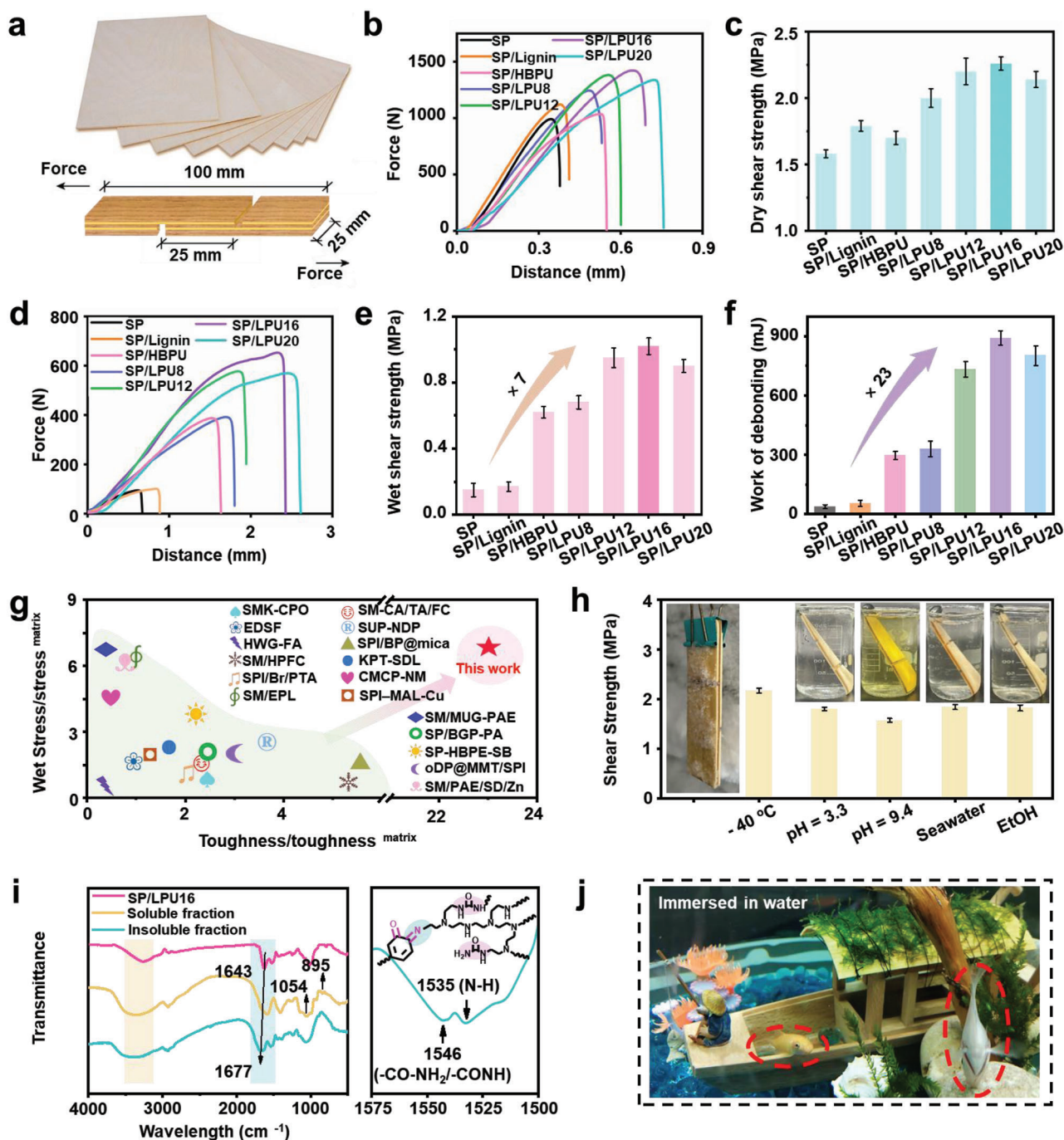MATERIALS**

www.afm-journal.de

Figure 2. a) Plywood prepared by SP/LPU adhesives, and schematic illustration of three-layer adhesive-bonded plywood specimens used for adhesion performance tests. b) Force-Distance curves of shear strength in dry environment. c) Dry shear strengths of plywood. d) Force-Distance curves on shear strength test performed in 63 °C hot water. e) Wet shear strength of plywood. f) The work of debonding of SP-based adhesives. g) The mechanical and water resistance enhancement of SP/LPU is far superior to that of protein-based composites prepared by other strategies. h) SP/LPU16 bonding capability in other different environments. i) FT-IR of water-resistant components of SP/LPU16. j) Boats made of SP/LPU16 bonded beech planks submerged underwater after one week.

water, with results shown in Figure 2b–d. SP only provides dry shear strength (Figure 2c) of 1.58 MPa and wet shear strength (Figure 2e) of 0.15 MPa, which are insufficient for practical applications. By varying the ratio of SP and LPU, the optimum LPU content of SP/LPU adhesive is uncovered at 16 wt.%

(SP/LPU16), with peak dry and wet shear strengths reached at 2.26 and 1.04 MPa ($p < 0.01$), which are nearly 1.5 and 7 folds of that for SP, respectively. When adding more LPU, the wet and dry shear strengths decrease to 0.9 and 2.14 MPa ($p < 0.01$), due to the insufficient quantity of SP to effectively dissipate

**ADVANCED
SCIENCE NEWS**

www.advancedsciencenews.com

**ADVANCED
FUNCTIONAL
MATERIALS**

www.afm-journal.de

mechanical energy and mitigate crack propagation. When SP and lignin (SP/lignin) are mixed and cured, a limited increase is found for the wet shear strength (0.3 MPa, $p < 0.01$), which demonstrates the poor waterproofing of SP and the limited reactivity of lignin.[21] The HBPU increase the dry and wet shear strength of SP adhesive to 0.62 and 1.7 MPa ($p < 0.01$), as more compact structure are induced by the hydrogen bonding and hyperbranched physical cross-linking between SP and HBPU. The cross-linking in SP/LPU facilitates the transfer and dissipation of stresses and external loads, thus significantly improving the cohesion strength of materials.

The SP/LPU also possesses superior fracture toughness under hot water. As a reference test, the fracture surfaces of SP-bonded plywood are found to be flat and smooth, owing to the typical brittle fracture. On the contrary, the plywood bonded with SP/LPU shows a rough fracture surface with explicit wood tearing and pull-out of fibre (Figure S9, Supporting Information), suggesting an improved adhesive strength and interfacial interaction. The debonding work calculated from the force-displacement curves (Figure 2d–f) indicates a relatively low value of 47.5 mJ for SP. Notably, SP/LPU presents an impressive combination of shear stress (1.04 MPa) and work of debonding (902 mJ), which are 7 and 23 folds of that from pristine SP ($p < 0.05$). This water-resistant mechanical performance enabled by bio-inspired structural design, is holistically compared with previously reports (Figure 2g; Table S1, Supporting Information). In addition, the mechanical properties of SP/LPU are superior to commercial urea-formaldehyde (UF),[33] phenolic resin (PF),[34] lignin-based (FPL)[2a] adhesives.

The solvent resistance is assessed by immersing the SP/LPU16 bonded Plywood specimens in different media for 12 h (Figure 2h). The shear strength of samples are 1.84 ± 0.05 MPa (seawater), 1.8 ± 0.04 MPa (acidic water), 1.57 ± 0.04 MPa (alkali water), and 1.82 ± 0.06 MPa (EtOH), respectively. All samples retain their original strong adhesive capacity. Surprisingly, the specimen presents a shear strength of 2.17 ± 0.05 MPa after storing at ultra-low temperature (−40 °C) for a week. The lap shear tests are performed on a variety of substrates (Figure S9, Supporting Information), where the results show strong adhesion of SP/LPU16 to different materials, including metals, glass, ceramics, and their combinations (Figure S10, Supporting Information). We also show the application of SP/LPU repair ceramics (Figure S11, Supporting Information). The bonded ceramic container has the application scenario of water resistance and low-temperature resistance. It can still not permeate water after holding water for 12 h and can also remain intact after storage at ultra-low temperature (−40 °C) for a week. Therefore, the SP/LPU adhesive can be used in repair industry, packaging industry, construction industry, woodworking industry, etc., and has a wide range of application scenarios.

We then assess the water resistance for SP/LPU16 adhesive by immersing the sample in hot water for 3 h (Figure 2i). The soluble fraction mainly consists of soy polysaccharides with characteristic absorption peaks at 1054 cm^{-1} corresponding to rhamnogalacturonan and 895 cm^{-1}, inferring the β-glyosidic ring.[35] The insoluble fraction exhibits an absorption peak corresponding to the urea group (1546 cm^{-1}) and imine structure (1535 cm^{-1}).[36] The rigor bonding performance can be attributed to strong cohesive strength and efficient load transfer caused by the

reticulated interconnected network of SP/LPU and the excellent stability enabled by the combination of imine and urea bonds (—NH—CO—NH—).

We also demonstrate the impressive water resistance bonding of SP/LPU16 adhesive (Figure 2j), by utilizing it to build a boat with beech-glued veneer (see assembly process in Figure S12, Supporting Information) and testing it in water. When the boat is immersed in water for a week, the structural integrity is well maintained with no environmental toxicity to the fish that live nearby. As being well-known, most petroleum-derived adhesives release volatile organic compounds (VOC), which cause skin irritation and respiratory toxicity to people.[15] The SP/LPU16 adhesive bonded board presents a relative VOC content of ≈4.6 × 10^6 mg m^{-2}, which is less than half of the commercialized epoxy adhesive and meets the E0 level (Table S2, Supporting Information). Besides, SP/LPU is 100% water-based without aldehyde components, so there is no cellular and biological toxicity, which is promising for biomedical and domestic applications.

2.3. Enhancement Mechanism of SP/LPU Adhesives

We next observe the development of cracking of notches between the cured adhesive block under SEM (**Figure 3a**), to understand the reinforcement and toughening mechanism. The SP sample presents a flat crack path that is almost parallel to the direction of applied stress (vertical orientation in the image), indicating a brittle fracture. However, the result in SP/LPU sample contains a mixed pack of message, including crack deflection, interfacial delamination, and crack branching. The crack deflection and branch normally indicate a stabilization and slow down the extension due to the increase of encountered energy barrier.[37] The interfacial delamination is mainly caused by the mechanical stiffness of connection structure and strong interfacial interactions.[38] When SP/LPU is stretched, the LPU skeleton is constrained by the bi-dynamic cross-linking of SP molecules, enabling the extension and alignment. This is due to the dissipative network mode of the external energy/load such as stable crack propagation, which can effectively delay and suppress the failure load.[39] This fracture mechanism is similar to that of dragonfly wings, which effectively improves the fracture toughness of the composite. In addition, strong intermolecular sacrificial hydrogen bonds further optimize the toughness of the adhesive.

A 2D numerical analysis is carried out by calculating the total fracture toughness (Γ_{total}) of SP/LPU adhesive with $\Gamma_{total} = \Gamma_0 + \Gamma_{diss}$ where Γ_0 is the intrinsic fracture energy of SP matrix and Γ_{diss} is the additional dissipated energy due to the sacrificial hydrogen bonding in the LPU skeleton (Figure 3b). The fracture energies are shown in Figure 3c with the diagrammatically illustrated experimental setting.[40] Without embedding the LPU skeleton, the fracture toughness of SP adhesive is as low as 0.85 kJ m^{-2} (equal to the fracture energy of SP), which means a weak resistance from SP chains to external force and low energy needed to break a layer of SP chains at the crack tip (Zone A in Figure 3b). After adding the LPU skeleton, a damage zone near the crack tip is formed (Zone B in Figure 3b) through the bi-dynamic cross-linking between the SP and LPU chains. The LPU
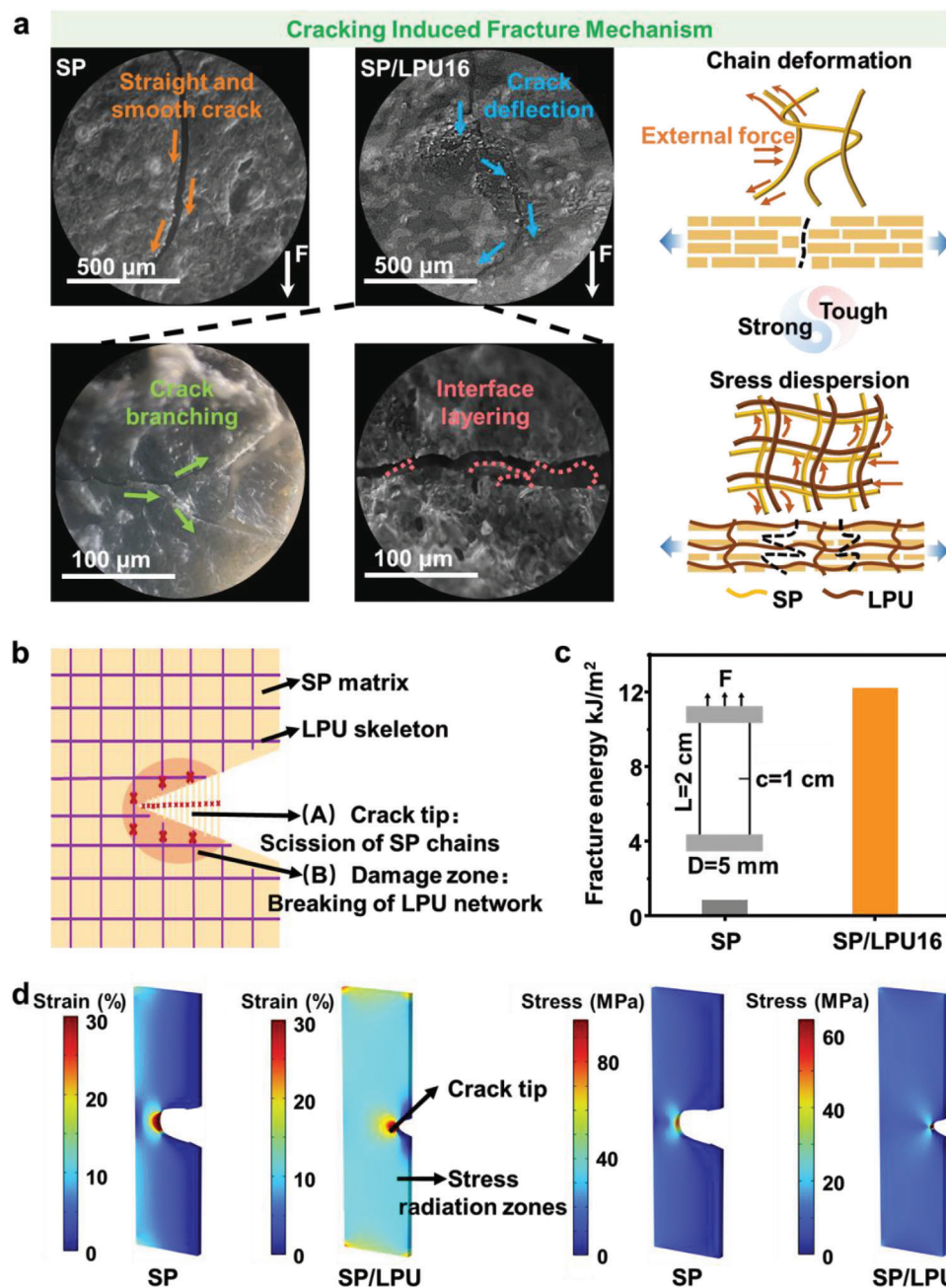
ADVANCED
SCIENCE NEWS

www.advancedsciencenews.com

ADVANCED
FUNCTIONAL
MATERIALS

www.afm-journal.de

Figure 3. a) Cross-sectional analysis of SP-based adhesives fracture. b) Enhanced toughening mechanism of SP/LPU adhesive. c) Fracture energy of SP-based adhesive layers. d) Finite elements analysis (FEA) simulations of stress distribution near the crack for pristine SP and SP/LPU16 adhesive films.

network dissipates substantial energy and toughens the SP/LPU composite, thus leading to a magnitude higher fracture energy of 12.2 kJ m^{-2}. This toughening mechanism is similar to the one in the double-network hydrogels, where the second sacrificial network is introduced to dissipate the mechanical energy and enhance the fracture toughness.[41]

Finite Element Analysis (FEA) is performed to further elucidate the strain localization at the crack tip (Figure 3d; Figure S13, Supporting Information). For SP, intensive strain localization/stress concentration is discovered at the crack tip to acceler-ate the crack extension and initiate the fracture. For SP/LPU, an effective energy dissipation can be observed at the nearby area of the crack tip, resulting in a reduced stress concentration at the crack tip. This is attributed to the mechanical rigidity of LPU structure and its strong interfacial supramolecular interactions. It should be noted that the above analysis is mostly based on 2D perspectives, as the adhesive layer is sandwiched between the plywood layers in the following engineering application with a high width/thickness aspect ratio over 50 (square plywood plates are used).
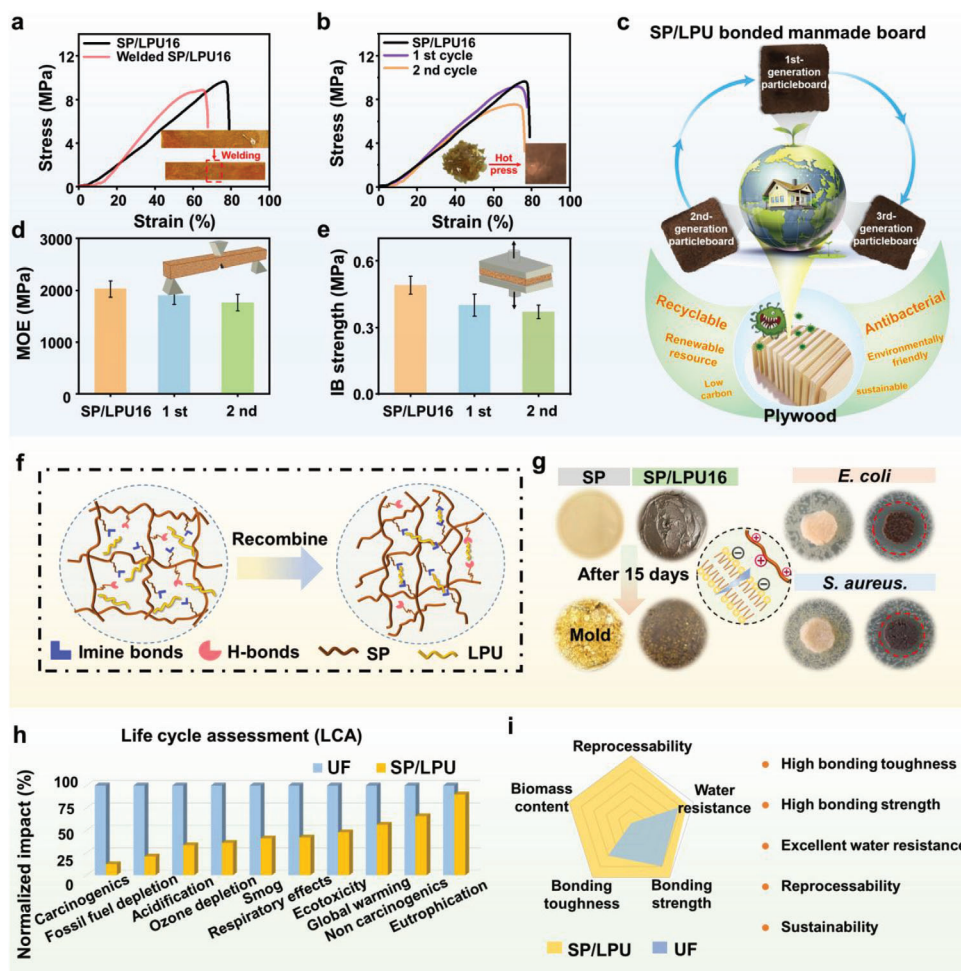
Figure 4. Stress–strain curves of adhesive samples from a) welding process and b) restoration from fragmental pieces. (The thickness of the film in Figure 4a is 0.02 mm, and the thickness of the reconstituted film in Figure 4b is 0.014 mm) c) Diagram of the reprocessing properties of SP/LPU-bonded particleboard. d) Modulus of elasticity (MOE), and e) internal bonding strength (IB) of SP/LPU-bonded recycled particleboard. f) Illustration of the restoration of bonds within SP/LPU during reprocessing. g) Observations of Mold behavior for adhesives under constant temperature and humidity, and the development of inhibition zone of adhesives toward *S. aureus* and *E. coli*. h) Life cycle assessment (LCA) of urea-formaldehyde resin (UF) and SP/LPU adhesive. i) Comparison of reprocessability, cost, and environmental impact between SP/LPU adhesive and commercial UF adhesive.

2.4. SP/LPU Adhesives Enabled Excellent Reprocessability and Recyclability of Bonded Board

To demonstrate the reprocessibility, we cut the SP/LPU adhesive stripe into half, wetted with water, and then overlapped before being hot-pressed at 140 °C and 4 MPa to weld two together. Tensile tests (**Figure 4a**) reveal that the welded SP/LPU strip possess a good retention of mechanical properties. Through a 10 min hot process with the same condition as shown above, the SP/LPU adhesive film can be restored from a fragmented state (Figure 4b). The stress–strain curve for recycled samples unveils a well-maintained shape that almost match with the original film. During reprocessing, the hyperbranch LPU with high mobility and reorganization ability accelerates the interpenetration and diffusion at the interface to promote the rearrangement of dynamic network (Figure 4f).[42]

Recycling end-of-life wood panel products (WP) has been one of the core sustainable targets for the industry.[43] Urea-formaldehyde (UF) resin adhesives have been prevalent in particleboard manufacturing but pose challenges to recyclability due to the difficulty of removing or reactivating them.[44] The SP/LPU adhesives appears to be a good alternative. As shown in Figure 4c, we fabricate the first-generation particleboard by crushing plywood into pellets with normal sizing amount adhesives and hot pressing, then crush and add SP/LPU adhesive based on 50 wt.% of normal sizing amount to create second-generation particleboard, then repeated to produce the third-generation particleboard. The modulus of elasticity (MOE, Figure 4d) and internal bonding strength (IB, Figure 4e) values of recycled particleboard are tested and compared. It is found that the MOE (1.760 GPa, $p < 0.05$) and IB (0.37 MPa, $p < 0.05$) of the third-generation particleboard remain ≈80% and 78% of the MOE (2.225 GPa), and IB (0.48 MPa) of the first-generation particleboard. In contrast, the MOE of UF-bonded particleboard after second-generation recycling is <40% of its first-generation.

**ADVANCED
SCIENCE NEWS**

www.advancedsciencenews.com

**ADVANCED
FUNCTIONAL
MATERIALS**

www.afm-journal.de

Moreover, the biomass-based SP adhesive shows extensive mycelial growth with >90% of the infected area after 15 days in a high-humidity environment (Figure 4g). The antimicrobial activity of SP/LPU adhesives is explored by selecting gram-negative (*Escherichia coli*) and gram-positive (*Staphylococcus aureus*) bacteria. The diameter of inhibition circle of SP/LPU adhesives against cationic *S. aureus* (2 mm) is smaller than that of the inhibition circle against anionic *E. coli* (4 mm), indicating that the adhesive has stronger antimicrobial activity against *E. coli*. This is mainly because the positively charged urea group in LPU interacts with the cell wall and DNA of anionic bacteria through non-covalent bonding, destroying the integrity of cell membrane and achieving better antibacterial effects.[45] In addition, the presence of Schiff base can bind to the ribosomes of bacteria, thus achieving the effect of inhibiting the growth and reproduction of bacteria.[46]

We also conduct a cradle-to-gate life cycle assessment (LCA) for SP/LPU and UF adhesives (Figure 4h; Table S3, Supporting Information), where the environmental impacts of SP/LPU are lower than UF in all categories. The environmental benefits and overall high performance (high strength, excellent recyclability, and biodegradability, Figure 4i; Table S4, Supporting Information) makes SP/LPU as an attractive candidate in sustainable engineering applications. Moreover, the raw material cost of SP adhesives is ≈2420 RMB ton⁻¹ (≈346 USD ton⁻¹), which is lower than the currently widely used UF resin (2800 RMB ton⁻¹ or 400 USD ton⁻¹), making them a promising alternative to traditional wood adhesive. Finally, a comparison chart reveals the advantages of SP/LPU in terms of bond strength, release, bio-based source, water resistance, and recyclability. SP/LPU exhibits superior performance to UF resin adhesives (Table S5, Supporting Information) and represents a significant advancement in the design of fully sustainable, strong, and tough high-performance adhesives for a more environmentally friendly and sustainable future.

3. Conclusion

We describe a dragonfly wing-inspired approach to achieve strong and tough bio-adhesive facilitated by structural processing and chemical cross-linking techniques. The SP bonding layer with a LPU mechanical framework formed a dual dynamic network consisting of gradient hydrogen and imine bonds. Through this unique assembly pattern and interfacial interactions, the brittle polymer cracking can be mitigated. The water resistance and fracture toughness of SP/LPU adhesive are 7 folds and 23 folds than these of SP based adhesive. Moreover, the dynamic network of adhesive allows for efficient diffusion and rearrangement at the interface, offering excellent recyclability and reprocessability. The recycled third-generation particleboard maintain a high stiffness of 1.760 GPa, which is ≈80% of the first-generation particleboard. This bio-adhesive strategy shed a light on the future development of eco-friendly alternative to the conventional petrochemical adhesive, to achieve strategic sustainability, including net zero emissions and the advancement of circular economy.

4. Experimental Section

Materials: Soybean protein (SP) with a protein content of at least 53 and 33 wt.% carbohydrates, and 7 wt.% water was supplied by China Shan-

dong Yuwang Group Co., Ltd. Enzymatic lignin was sourced from Shandong Longli Biotechnology Co., Ltd. Anhydrous ferric chloride (FeCl₃, 99%, AR), urea (99%, AR), and polyethyleneimine (PEI, 50% aqueous solution, Mw = 1800, 99%, AR) were supplied by Shanghai Macklin Biochemical Technology Co., Ltd. All solvents and reagents were used as received.

Synthesis of LPU: In the first step, hyperbranched polyurea (HBPU) was obtained through a one-pot method polycondensation reaction. This involves combining urea and PEI in a 250 mL round bottom flask, in a 3:1 molar ratio, which was then stirred at 135 °C for 10 h. The ammonia produced during the process was trapped in a water bath. The next step entails adding 5 mL (5 wt.%) of FeCl₃ solution to a lignin suspension (5 g, 50 wt.%) and adjusting the pH to 9 using a 10 M NaOH solution. This was stirred for 2 h to form a uniform moisture dispersion. The two aqueous dispersions (The solid mass ratio of oxidized lignin to HBPU was 1:1.5) were then mixed and stirred at 60 °C for 30 min, and finally obtained LPU suspension.

Preparation of SP/LPU Adhesive: The creation process for the SP/LPU x adhesive involves first dissolving 28 g of SP in water (70 mL), followed by 600 s of stirring to ensure proper distribution. A specified quantity of LPU was then mixed into the aqueous medium, and stirring continued for another 60 s. The value of x denotes the percentage of LPU mass based on SP. The sample of SP/lignin was prepared by adopting the same methodology.

Characterization: The Fourier Transform infrared spectroscopy (FT-IR) spectrometer (Nicolet 6700, Thermo Fisher Scientific, USA) with a was used to analyze FT-IR spectra of all specimens between 400 and 4000 cm⁻¹. High-resolution ¹³C nuclear magnetic resonance (NMR) spectra (DSX-300, Agilent) was taken on at 600 MHz. A Q 150R S plus rotary pumped coater (30 s plus 20 mA) was used to coat the samples prior to scanning electron microscopy (SEM) images of the LPU. In order to prepare the samples, granular water dispersions were dropped onto a carbon film grid and the excess water was absorbed with filter paper. The cured adhesive surfaces were examined using a Phenom scanning electron microscope (Phenom Pure G5). The grafting rate was determined using a TA Instruments Q50 Thermogravimetric analyzer under nitrogen. The samples were heated from 25 °C to 650 °C in N₂ with a heating rate of 20 °C min⁻¹. X-ray photoelectron spectroscopy (XPS) data were collected via AXIS Ultra DLD, Shimadzu (UK) with Al-Kα radiation. A RIGAKU Ultima IV X-ray diffractometer manufactured in Japan with Cu K radiation was used to gather X-ray diffraction (XRD) data from 5° to 60°. The zeta potential and particle size of the LPU nanoparticles samples were measured by adopting a nanoparticle size and zeta potential analyzer (Zetasizer Nano ZS90, UK). The samples were diluted to 1 wt.% dispersion with a neutral pH. The storage modulus and viscosity of the adhesives were quantified using a Brookfield rotational viscometer (DV-II, Middleboro) at room temperature within 0–150 s⁻¹. The plates were cut into thin specimens with dimensions of 50 mm (length) × 10 mm (width) × 2 mm (thickness) for Dynamic mechanical analysis (DMA), using a three-point loading bending method with an amplitude of 60 μm, a loading frequency of 1 Hz, a temperature range of 25–20 °C, and a temperature increase rate of 5 °C min⁻¹. Volatile organic compounds (VOCs) were collected on the gas chromatograph/mass spectrometer (GC/MS, QP2010 ultra, Shimadzu, Japan).

Bonding Strength Test: The shear strength of three-ply poplar plywood was used to assess the bonding strength of SP-based adhesives. In accordance with the earlier study, three-ply plywood measuring 200 mm × 200 mm × 4.5 mm and having an adhesive spreading rate of 180 g m⁻² (for a single veneer side) might be put together in a crisscross pattern and hot pressed for 320 s at 120 °C and 1.0 MPa. The plywood was cooled at room temperature for 1 day prior to testing. Using an AGS-X electronic universal testing machine (Shimadzu, Japan), plywood samples were quantified for shear strength at a speed of 10 mm min⁻¹ according to GB/T 17657-2013. The shear strength of six specimens was tested dry, while the shear strength of six additional specimens was tested after soaking in water at 63 °C ± 3 °C for 3 h before testing.

The adhesion performance and water resistance of the adhesives were evaluated by measuring the dry (for applications in dry environments) and wet (for applications in humid environments) adhesion strengths and toughness of three-layer plywoods prepared with adhesives. Specifically, the shear strength was defined as the maximum force (in N) of the

2406557 (8 of 10)

**ADVANCED
SCIENCE NEWS**

www.advancedsciencenews.com

**ADVANCED
FUNCTIONAL
MATERIALS**

www.afm-journal.de

adhesive joint divided by the overlap area (in mm^2), the peel work of plywoods was defined as the integral of the force-distance curve (in mJ).

Residual Rate Test: The cured adhesive was dried at 120 °C until its mass (M) was constant, immersed in water at 60 °C for 6 h, and then dried at 105 °C until another constant weight (m). The residual rate was calculated as m/M×100%.

Bonding Strength Testing of Different Substrates: The lap shear adhesion of various substrates was assessed using specimens made of ceramic, steel, wood, and glass with dimensions of 25 mm × 76 mm. A uniform application of 0.2 g of adhesive was administered onto a substrate with a 25 mm × 25 mm overlap area. Subsequently, a 6 min curing process was carried out at a pressure of 120 °C and 1 MPa. Following the cooling process, a lap shear test was conducted.

Reprocessability Test: The solution was poured onto the mold and prepared a cured adhesive film at 140 °C and 4 MPa for 4 min. All samples were cut into rectangular strips 80 mm long and 10 mm wide and placed at 25 °C and 50% relative humidity for a week before tensile testing. The tensile strength and elongation fracture were directly assessed on Shimadzu AGS-X electronic universal testing machine at a crosshead speed of 10 mm min^{-1}. Each sample was tested at least three times. The films were cut off and then immersed soak the joint in water at 80 °C for 10 min, and then regenerated the recovered film by hot pressing at 140 °C and 4 MPa. The same method was used to evaluate recoverability according to tensile strength.

Approximately 170 g of wood particles crushed from plywood and 200 g of SP/LPU16 adhesive were mixed in a blender for 10 min, then adhesive-coated wood chips were placed in ventilated oven (60 °C) overnight until the moisture content reached 10%. The materials were poured into a stainless-steel mold and subjected to hot-pressed them at 150 °C for 13 min to make first-generation particleboard (5 mm in thickness and 1.0 g cm^{-3} in density). Approximately 170 g of wood chips were pulverized from the first and second generation particleboard, and LPU based on 10% of the normal sizing amount was added respectively to manufacture the second and third generation particleboard according to the same method.

The mechanical properties included modulus of elasticity (MOE) and internal bonding strength (IB) strength were carried out according to the GB/T 17657–2013 standard. Samples with a size of 200 mm × 50 mm x 7.5 mm were cut from each panel for MOE tests. The Instron Tensile Machine (AGS-X) was used with a crosshead speed of 10 mm min^{-1}. The Span of supporting beam was 120 mm and a load was applied at the center of the sample. Besides, samples with a size of 50 mm × 50 mm x 7.5 mm were cut from each panel for IB test.

Mildew Resistance and Antibacterial Tests: Ten g of adhesive samples were loaded into Petri dishes and subsequently placed in an incubator under conditions of 90% relative humidity and 30 °C. The progression of mildew on the adhesive samples was monitored through a camera.

The present study investigated the antibacterial efficacy of SP-based adhesives toward both gram-negative *Escherichia coli* (*E. coli*) and gram-positive *Staphylococcus aureus* (*S. aureus*) bacteria. The paper diffusion approach was employed to gauge the inhibitory effects of the adhesives. Bacterial suspensions of *E. coli* and *S. aureus* were diluted to 108 (CFU) mL^{-1}, and LB agar was used as the medium for bacterial inoculation. Prior to testing, adhesive samples with a diameter of 5 mm were exposed to ultraviolet radiation for 300 min. The adherent specimens were incubated for 1 day at 37 °C by placing them on the prepared LB agar, following which, the inhibition zones diameters were measured, and photographs were taken.

Life Cycle Assessment (LCA) Analysis: The LCA is conducted by following the environmental impact assessment methodology set forth in the international ISO 14 040 standard. The modeling process of the adhesives production process used open LCA 1.11.0 software, the U.S. Life Cycle Inventory (USLCI) and the Ecoinvent 3 databases, and the TRACI (version v2.1) methodology to assess their environmental impact. The quantitative results of LCA of the PF and SP/LPU adhesives are shown in Tables S4 (Supporting Information). The quantitative results were normalized in bar charts produced for a more visual comparison.

Finite Elements Analysis (FEA): The variation of stress and strain distribution during fracture of the specimen was studied by finite ele-

ment method. All simulations were performed using commercial software COMSOL 6.1. The fracture mechanism was qualitatively revealed by using a structural model with the same size as the experimental sample in Figure 4b. All used parameters are shown in Table S5 (Supporting Information).

Statistical Analysis: At least six samples of each test were performed. The quantitative data were expressed as mean ± standard deviation and analyzed by IBM SPSS Statistics 26. The two-tailed t-tests (independent samples test) for dry/wet shear strength and peel work of the adhesives in the manuscript was performed, and the statistical difference was set at $p < 0.05$.

Supporting Information

Supporting Information is available from the Wiley Online Library or from the author.

Acknowledgements

Conflict of Interest

The authors declare no conflict of interest.

Author Contributions

Y.Z. and J.L. contributed equally to this work. Y.Z., J.Z., and J.L. conceived the research idea. Y.Z., J.L., S.G., and B.X. designed the experiments and wrote the manuscript. Q.J., S.C., Z.G., and B.X. performed the theoretical analysis. S.G. and J.L. performed the experiments and collected the data. J.L., X.H., and B.X. supervised the project. All authors read and approved the final manuscript.

Data Availability Statement

The data that support the findings of this study are available in the supplementary material of this article.

Keywords

[1] C. R. Westerman, B. C. McGill, J. J. Wilker, *Nature* **2023**, *621*, 306.

[2] a) G. Yang, Z. Gong, X. Luo, L. Chen, L. Shuai, *Nature* **2023**, *621*, 511; b) Q. Xia, C. Chen, Y. Yao, J. Li, S. He, Y. Zhou, T. Li, X. Pan, Y. Yao, L. Hu, *Nat. Sustainability* **2021**, *4*, 627.

**ADVANCED
SCIENCE NEWS**

www.advancedsciencenews.com

**ADVANCED
FUNCTIONAL
MATERIALS**

www.afm-journal.de

[3] X. Zhang, C. Long, X. Zhu, X. Zhang, J. Li, J. Luo, J. Li, Q. Gao, *ACS Nano* **2023**, *17*, 18850.

[4] J. K. Román, J. J. Wilker, *J. Am. Chem. Soc.* **2018**, *141*, 1359.

[5] T. Todorovic, E. Norström, F. Khabbaz, J. Brücher, E. Malmström, L. Fogelström, *Green Chem.* **2021**, *23*, 3322.

[6] a) Z.-H. Wang, B.-W. Liu, F.-R. Zeng, X.-C. Lin, J.-Y. Zhang, X.-L. Wang, Y.-Z. Wang, H.-B. Zhao, *Sci. Adv.* **2022**, *8*, eadd8527; b) M. G. Mazzotta, A. A. Putnam, M. A. North, J. J. Wilker, *J. Am. Chem. Soc.* **2020**, *142*, 4762.

[7] a) H. S. Wang, X. Y. Shi, Y. T. Xie, S. S. Gao, Y. Dai, C. H. Lai, D. H. Zhang, C. P. Wang, Z. H. Guo, F. X. Chu, *Cell Rep. Phys. Sci.* **2023**, *4*, 194; b) P. Sun, S. Mei, J. F. Xu, X. Zhang, *Adv. Sci.* **2022**, *9*, 2203182; c) Z. Su, L. Yu, L. Cui, G. Zhou, X. Zhang, X. Qiu, C. Chen, X. Wang, *ACS Nano* **2023**, *17*, 21420.

[8] G. W. Zhou, H. S. Zhang, Z. P. Su, X. Q. Zhang, H. A. Zhou, L. Yu, C. J. Chen, X. H. Wang, *Adv. Mater.* **2023**, *35*, 2301398.

[9] a) W. Li, X. Liu, Z. Deng, Y. Chen, Q. Yu, W. Tang, T. L. Sun, Y. S. Zhang, K. Yue, *Adv. Mater.* **2019**, *31*, 1904732; b) Z. Guo, X. Lu, X. Wang, X. Li, J. Li, J. Sun, *Adv. Mater.* **2023**, *35*, 2300286.

[10] a) B. H. Cheng, J. H. Yu, T. Arisawa, K. Hayashi, J. J. Richardson, Y. Shibuta, H. Ejima, *Nat. Commun.* **2022**, *13*, 1892; b) Z. H. Zhao, P. C. Zhao, Y. Zhao, J. L. Zuo, C. H. Li, *Adv. Funct. Mater.* **2022**, *32*, 2201959.

[11] a) T. Liu, C. L. Li, H. Yao, F. Y. Sun, L. Wang, B. W. Yao, J. H. Xu, J. J. Fu, *Mater. Horiz.* **2023**, *10*, 2968; b) Y. Huang, D. R. King, T. L. Sun, T. Nonoyama, T. Kurokawa, T. Nakajima, J. P. Gong, *Adv. Funct. Mater.* **2017**, *27*, 1605350.

[12] a) W. Huang, D. Restrepo, J. Y. Jung, F. Y. Su, Z. Liu, R. O. Ritchie, J. McKittrick, P. Zavattieri, D. Kisailus, *Adv. Mater.* **2019**, *31*, 1901561; b) X. Liang, G. Chen, I. M. Lei, P. Zhang, Z. Wang, X. Chen, M. Lu, J. Zhang, Z. Wang, T. Sun, *Adv. Mater.* **2023**, *35*, 2207587.

[13] G. Zeng, J. T. Aladejana, K. Li, Q. Xue, Y. Zhou, J. Luo, Y. Dong, X. Li, J. Li, *Int. J. Biol. Macromol.* **2023**, *253*, 127669.

[14] X. Liu, L. X. Shi, X. Z. Wan, B. Dai, Y. P. Chen, S. T. Wang, *ACS Mater. Lett.* **2021**, *3*, 1453.

[15] Y. Wang, E. J. Jeon, J. Lee, H. Hwang, S. W. Cho, H. Lee, *Adv. Mater.* **2020**, *32*, 2070326.

[16] J. H. Xu, T. Liu, Y. Z. Zhang, Y. N. Zhang, K. Wu, C. X. Lei, Q. Fu, J. J. Fu, *Matter* **2021**, *4*, 2474.

[17] a) Y. Wei, H. Guo, S. Zhang, J. Li, Y. Wang, C. Liu, *J. Comput. Mech.* **2022**, *31*, 459; b) Z. Zhang, L. Zhang, Z. Yu, J. Liu, X. Li, Y. Liang, *Micron* **2018**, *110*, 67.

[18] S. Jongerius, D. Lentink, *Exp. Mech.* **2010**, *50*, 1323.

[19] V. Ibrahim, G. Mamo, P.-J. Gustafsson, R. Hatti-Kaul, *Ind. Crops Prod.* **2013**, *45*, 343.

[20] H. C. Hu, H. Xu, J. Wu, L. Li, F. Yue, L. Huang, L. Chen, X. Zhang, X. Ouyang, *Adv. Funct. Mater.* **2020**, *30*, 2001494.

[21] Y. Ma, Z. Kou, Y. Hu, J. Zhou, Y. Bei, L. Hu, Q. Huang, P. Jia, Y. Zhou, *Int. J. Adhes. Adhes.* **2023**, *126*, 103444.

[22] a) J. H. Xu, Y. K. Li, T. Liu, D. Wang, F. Y. Sun, P. Hu, L. Wang, J. Y. Chen, X. B. Wang, B. W. Yao, J. J. Fu, *Adv. Mater.* **2023**, *35*, 2300937; b) S. Ghosh, S. Ramakrishnan, *Angew. Chem., Int. Ed.* **2004**, *43*, 3264; c) X. B. Zhu, W. J. Zhang, G. M. Lu, H. C. Zhao, L. P. Wang, *ACS Nano* **2022**, *16*, 16724.

[23] C. Wang, M. Fadeev, M. Vazquez-Gonzalez, I. Willner, *Adv. Funct. Mater.* **2018**, *28*, 1803111.

[24] a) V. Basavalingappa, T. Guterman, Y. M. Tang, S. Nir, J. T. Lei, P. Chakraborty, L. Schnaider, M. Reches, G. H. Wei, E. Gazit, *Adv. Sci.* **2019**, *6*, 1900218; b) M. A. Ramin, L. Latxague, K. R. Sindhu, O. Chassande, P. Barthelemy, *Biomaterials* **2017**, *145*, 72; c) J. Liu, C. S. Y. Tan, Z. Yu, N. Li, C. Abell, O. A. Scherman, *Adv. Mater.* **2017**, *29*, 1605325.

[25] Z. Q. Zhang, D. Lei, C. X. Zhang, Z. Y. Wang, Y. H. Jin, W. Zhang, X. K. Liu, J. Q. Sun, *Adv. Mater.* **2023**, *35*, 2208619.

[26] H. Xu, S. Zhao, A. Yuan, Y. Zhao, X. Wu, Z. Wei, J. Lei, L. Jiang, *Small* **2023**, *19*, 2300626.

[27] S. Hao, R. Dai, Q. Fu, Y. Wang, X. Zhang, H. li, X. Liu, J. Yang, *Adv. Funct. Mater.* **2023**, *40*, 2302840.

[28] Q. Xia, C. Chen, Y. Yao, S. He, X. Wang, J. Li, J. Gao, W. Gan, B. Jiang, M. Cui, *Adv. Mater.* **2021**, *33*, 2001588.

[29] Y. Deng, Q. Zhang, C. Shi, R. Toyoda, D.-H. Qu, H. Tian, B. L. Feringa, *Sci. Adv.* **2022**, *8*, eabk3286.

[30] Y. Zhou, Z. Fang, G. D. Zeng, Z. J. Tang, F. D. Zhang, J. Luo, X. O. Li, K. Li, J. Z. Li, *Chem. Eng. J.* **2022**, *436*, 135023.

[31] S. Jiang, Y. Wei, S. Q. Shi, Y. Dong, C. Xia, D. Tian, J. Luo, J. Li, Z. Fang, *Nano Lett.* **2021**, *21*, 3254.

[32] M. H. Hussin, N. H. Abd Latif, T. S. Hamidon, N. N. Idris, R. Hashim, J. N. Appaturi, N. Brosse, I. Ziegler-Devin, L. Chrusiel, W. Fatriasari, F. A. Syamani, A. H. Iswanto, L. S. Hua, S. Al Edrus, W. C. Lum, P. Antov, V. Savov, M. A. R. Lubis, L. Kristak, R. Reh, J. Sedliacik, *J. Mater. Res.* **2022**, *21*, 3909.

[33] L. Chen, Q. Gao, J. Zhang, H. Chen, S. Zhang, J. Li, *BioResources* **2014**, *9*, 2975.

[34] H. Y. Kordkheili, A. Pizzi, *Eur. J. Wood Wood Prod.* **2021**, *79*, 199.

[35] Y. T. Dong, Z. L. Rao, Y. C. Liu, X. J. Zheng, K. Y. Tang, J. Liu, *Food Packag. Shelf Life* **2023**, *35*, 101039.

[36] a) S. S. Jada, *J. Appl. Polym. Sci.* **1988**, *35*, 1573; b) J. Sun, H. He, K. Zhao, W. Cheng, Y. Li, P. Zhang, S. Wan, Y. Liu, M. Wang, M. Li, *Nat. Commun.* **2023**, *14*, 5348.

[37] M. Wang, S. Shi, J. Fineberg, *Science* **2023**, *381*, 415.

[38] X. Yue, H. B. Yang, Z. M. Han, Y. X. Lu, C. H. Yin, X. Zhao, Z. X. Liu, Q. F. Guan, S. H. Yu, *Adv. Mater.* **2023**, *36*, 2306451.

[39] Y. Wang, X. Huang, X. Zhang, *Nat. Commun.* **2021**, *12*, 1291.

[40] Z. Zhang, G. Chen, Y. Xue, Q. Duan, X. Liang, T. Lin, Z. Wu, Y. Tan, Q. Zhao, W. Zheng, *Adv. Funct. Mater.* **2023**, *33*, 2305705.

[41] a) J. P. Gong, *Soft Matter* **2010**, *6*, 2583; b) X. Kuang, M. O. Arıcan, T. Zhou, X. Zhao, Y. S. Zhang, *Acc. Mater. Res.* **2022**, *4*, 101.

[42] Y. Zhang, H. Yan, R. Yu, J. Yuan, K. Yang, R. Liu, Y. He, W. Feng, W. Tian, *Adv. Sci.* **2024**, *11*, 2306350.

[43] C. K. de Carvalho Araújo, M. B. Ferreira, R. Salvador, C. K. C. de Carvalho Araújo, B. S. Camargo, S. K. D. C. A. Camargo, C. I. de Campos, C. M. Piekarski, *J. Cleaner Prod.* **2022**, *355*, 131729.

[44] Y. Zhou, Z. Fang, G. Zeng, Z. Tang, F. Zhang, J. Luo, X. Li, K. Li, J. Li, *Chem. Eng. J.* **2022**, *436*, 135023.

[45] X. Ou, X. Y. Zou, Q. B. Liu, L. G. Li, S. C. Li, Y. H. Cui, Y. J. Zhou, F. Yan, *Chem. Mater.* **2023**, *35*, 1218.

[46] Q. Zhao, M. Zhang, S. Gao, Z. Pan, Y. Xue, P. Jia, C. Bo, Z. Luo, F. Song, Y. Zhou, *J. Mater. Chem. A* **2022**, *10*, 11363.